# Prediction of Transient Bed Height in Batch Sedimentation at Large Times

**Shane P. Usher and Peter J. Scales**
Particulate Fluids Processing Centre, Dept. of Chemical and Biomolecular Engineering, The University of Melbourne, Victoria, 3010, Australia

**Lee R. White**
Dept. of Chemical Engineering, Carnegie Mellon University, Pittsburgh, PA 15213

*DOI 10.1002/aic.10709*
*Published online October 28, 2005 in Wiley InterScience (www.interscience.wiley.com).*

*Sedimentation of particulate slurries in industrial sedimentation ponds and laboratory-based batch settling tests is difficult to describe analytically. Understanding long-time settling behavior is of particular importance when extrapolating existing sedimentation data to predict the final extent and how long it will take. A simple analytical equation has been derived to describe the final stage of compression in batch settling. In addition, numerical methods for determining the equation parameters have been proposed and demonstrated. The validity of the analytical equation and the parameters determined has been verified by comparison with finite element predictions. This new knowledge has the potential to significantly reduce the computational time requirements of predicting long-time batch settling behavior.* © 2005 American Institute of Chemical Engineers *AIChE J,* 52: 986–993, 2006

*Keywords: batch settling, sedimentation, consolidation, compressive yield stress, hindered settling function, dewaterability characterization*

## Introduction

Sedimentation of particulate slurries in industrial sedimentation ponds and laboratory based batch settling tests is industrially important, but not well understood, especially at long times. Industrial sedimentation ponds, with depths of 10 meters or more, are routinely filled with particulate slurries and then left to consolidate for years. In laboratory-based batch settling tests, the nominal equilibrium sediment-liquid interface height is often recorded at a predefined time, such as 1 or 24 hours, without any clear knowledge of whether sedimentation has actually ceased. In both cases, a predictive understanding of long-time batch settling behavior would be useful.

Material properties that describe the suspension network strength and resistance to flow of liquid through the network structure dictate dewatering behavior. The gel point, $\phi_g$, represents the solids concentration at which the suspension forms a continuously networked structure. Given material properties, such as the compressive yield stress, $P_y(\phi)$, and hindered settling function, $R(\phi)$, over the relevant range of solids concentrations, dewatering phenomena obey a partial differential equation that describes the variation of the solids volume fraction as a function of both space and time, $\phi(z,t)$ (see Eq. 6). Batch settling can be split into two general cases, where (i) $\phi(z,0) \leq \phi_g$ and (ii) $\phi(z,0) < \phi_g$.

For case (i), analytical solution of the PDE is achievable when the solids concentration is less than the gel point, $\phi_g$, using an analytic transform.[1,2] However, this method is only valid for the prediction of $h(t)$ until $\phi(h(t),t) = \phi_s < \phi_g$, where $\phi_s$ is the limit of applicability for the transform. The equilibrium solids concentration distribution at infinite time, $\phi(z,\infty)$, can also be determined. For other times, only computationally

Correspondence concerning this article should be addressed to P. J. Scales at peterjs@unimelb.edu.au.

intensive numerical algorithms are available, such as an upwind finite-difference scheme described by Bürger and Karslen.[3]

For case (ii), the initial rate of sedimentation, $h'(0)$, and equilibrium solids concentration distribution, $\phi(z,\infty)$, can be analytically determined, but the transient behavior must be computed numerically using an algorithm such as the Runge-Kutta shooting method described by Howells and co-workers.[4]

The limitation of the numerical algorithms described is that as the required accuracy increases, the required computation time becomes prohibitive. It would be more useful to have a closed functional form that adequately describes batch settling at large times. Roberts[5] demonstrated that the shape of the compression curve for experimental data exhibits logarithmic behavior, an assertion generally accepted by subsequent authors.[6,7] Piston-driven filtration behavior has been described analytically by Landman and White,[8] and an analogous derivation for the final stage of batch settling is presented here.

## Material Properties

As a prelude to introducing the mathematical theory, it is important to have a general understanding of the material properties that determine batch-settling behavior. The network strength is quantified in terms of the compressive yield stress, $P_y(\phi)$, which is, for a suspension at solids concentration $\phi$, the maximum compressive stress that can be applied before irreversible yielding and dewatering to a higher solids concentration. $P_y(\phi)$ is zero for all solids concentrations below $\phi_g$. The rate at which a material can be dewatered is quantified in terms of the hindered settling function, $R(\phi)$, which represents the resistance to flow through the suspension network structure and is inversely related to the traditional Darcian permeability $k_{Darcy}(\phi)$ according to the following equation[9]

$$k_{Darcy}(\phi) = \frac{\eta}{R(\phi)} \frac{1-\phi}{\phi}, \tag{1}$$

where $\eta$ is the liquid viscosity, as opposed to the slurry viscosity.

### *Material property characterization*

A detailed protocol for the quantification of the dewatering parameters to be used as inputs to the dewatering model has been established. The experimental techniques employed are generic to the assessment of dewatering performance in a range of industries. Techniques of relevance include batch-settling tests[10-12] for permeability analysis at low solids and for compressibility analysis at solids near the gel point and stepwise pressure filtration[13,14] for permeability and compressibility analysis at higher solids. Other techniques, including gravity permeation[12] and centrifugation,[10] have also been developed.

Once obtained, the experimental data can be fitted with curves such as those proposed by Landman and co-workers.[15] The most commonly utilized functional forms are given by:

$$P_y(\phi) = k\left(\left(\frac{\phi}{\phi_g}\right)^n - 1\right) \quad \text{for } \phi > \phi_g, \tag{2}$$

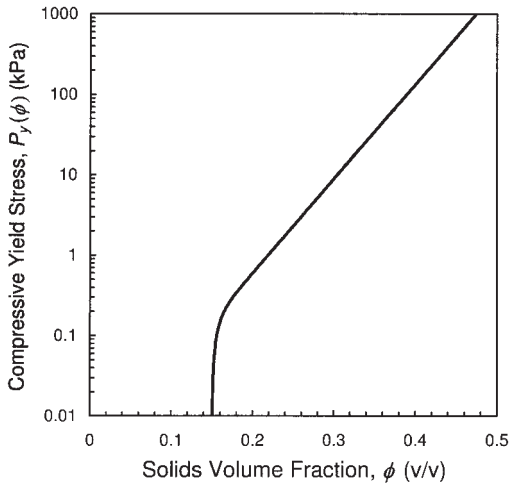


**Figure 1. Example of compressive yield stress, $P_y(\phi)$, curve using the asymptote and exponential-power law functional form given by Eq. 4 with parameter values $\phi_g = 0.15$, $p_a = 27$, $p_b = 1$, $p_m = 20$, and $p_n = 1$.**

$$R(\phi) = w(1-\phi)^m, \tag{3}$$

where $P_y(\phi) = 0$ for $\phi \le \phi_g$ and $k$, $n$, $w$ and $m$ are empirical fitting parameters. Unfortunately, these functional forms have been found to be too rigid and thus unable to provide an adequate fit to experimental data that span a wide range of solids concentrations.[12] Two alternatives shown to provide a better fit are:

$$P_y(\phi) = \left(1 - \left(\frac{\phi_g}{\phi}\right)^{p_m}\right) e^{(p_a\phi^{p_n}+p_b)} \quad \text{for } \phi > \phi_g, \tag{4}$$

$$R(\phi) = r_a(\phi - r_g)^{r_n} + r_b, \tag{5}$$

where $P_y(\phi) = 0$ for $\phi \le \phi_g$ and $p_a$, $p_b$, $p_m$, $p_n$, $r_a$, $r_b$, $r_g$ and $r_n$ are empirical fitting parameters. Generic curves using Eqs. 4 and 5 with parameters representative of an industrial mineral slurry are presented in Figures 1 and 2. Other potential alternatives include interpolation functions or composite functions that split the curve into a number of domains, each with its own parameter set.

## Theory

A schematic of a batch-settling test is shown in Figure 3. The apparatus includes a cylinder filled to height $h_0$ with a flocculated suspension of particles at an initial volume fraction $\phi_0 < \phi_g$. The liquid-sediment interface height, $h(t)$, decreases over time as the suspension consolidates towards the base of the cylinder. A bed, with solids concentration greater than the gel point, builds up at the base of the cylinder until time, $t_c$, when the solids volume fraction at the sediment-liquid interface is equal to the gel point, $\phi(h(t_c), t_c) = \phi_g$. For times greater than $t_c$, the bed consolidates towards the equilibrium solids concentration distribution, $\phi(z,\infty)$.

The variation of solids volume fraction with height from the

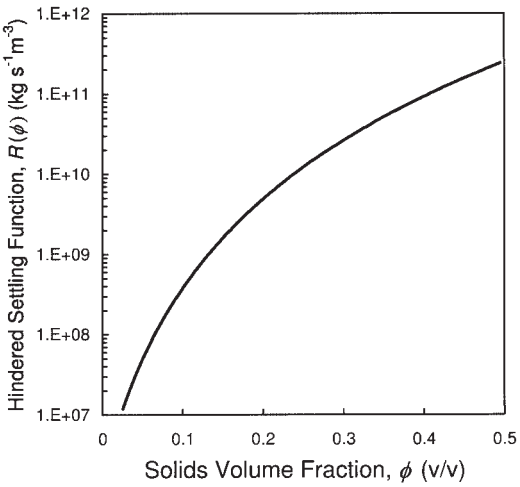


**Figure 2. Example of hindered settling function, $R(\phi)$, curve using the functional form given by Eq. 5 with parameter values $r_a = 5 \times 10^{12}$, $r_b = 0$, $r_g = -0.05$, and $r_n = 5$.**

base of the sediment, $z$, and time, $t$, is denoted by $\phi(z,t)$, with settling described by the equation

$$\frac{\partial \phi}{\partial t} = \frac{\partial}{\partial z}\left(D(\phi)\frac{\partial \phi}{\partial z} + U_{sed}(\phi)\phi\right), \tag{6}$$

where the downward sedimentation velocity

$$U_{sed}(\phi) = \frac{\Delta\rho g(1-\phi)^2}{R(\phi)}, \tag{7}$$

with $\Delta\rho$ being the difference in density between the solid and fluid and $g$ the gravitational acceleration. The hindered settling function

$$R(\phi) = \frac{\lambda}{V_p} r(\phi), \tag{8}$$

where $\lambda$ is the Stokes settling coefficient, $V_p$ is the particle volume, and $r(\phi)$ is the hindered settling factor that accounts for the deviation from Stokes law as the solids volume fraction increases ($r(0) = 1$). The volume fraction dependent solids diffusivity

$$D(\phi) = \left(\frac{dP_y(\phi)}{d\phi}\right)\frac{(1-\phi)^2}{R(\phi)}. \tag{9}$$

In batch settling, the differential equation given by Eq. 6 is subject to the boundary conditions

$$\left.\frac{\partial \phi}{\partial z}\right|_{z=0} = -\left.\frac{U_{sed}(\phi)\phi}{D(\phi)}\right|_{z=0} \tag{10}$$

and

$$\phi|_{z=h(t)} = \phi_g. \tag{11}$$

At time $t = \infty$ when the solids flux is zero everywhere, $\partial\phi/\partial t = 0$, the equilibrium solids concentration distribution $\phi(z, \infty) = \Phi(z)$ and the governing equation, Eq. 6, simplifies to

$$0 = D(\Phi)\frac{d\Phi}{dz} + U_{sed}(\Phi)\Phi. \tag{12}$$

This is equivalent to

$$\frac{dP_y(\Phi(z))}{dz} = -\Delta\rho g\Phi(z). \tag{13}$$

The compressive stress at the base of the sediment is

$$P_y(\phi_\infty) = \Delta\rho g\phi_0 h_0 \tag{14}$$

where

$$\phi_\infty = \phi(0, \infty). \tag{15}$$

Equation 13 can be transformed to give

$$\frac{d\Phi(z)}{dz} = -\frac{\Delta\rho g\Phi(z)}{P_y'(\Phi(z))}, \tag{16}$$

which is integrated from the base boundary condition $\Phi(0) = \phi_\infty$ to the top of the sedimented bed at point $z^*$ where $\Phi(z^*) = \phi_g$ to determine $h_\infty = h(\infty) = z^*$.

### *Scaling*

Introducing a length scale $L$, to be determined, we write:

$$H(T) = \frac{h(t)}{L}, \quad T = \frac{t}{\left(\frac{L}{U_{sed}(\phi_g)}\right)}, \quad Z = \frac{z}{L}, \tag{17}$$

then Eq. 6 becomes

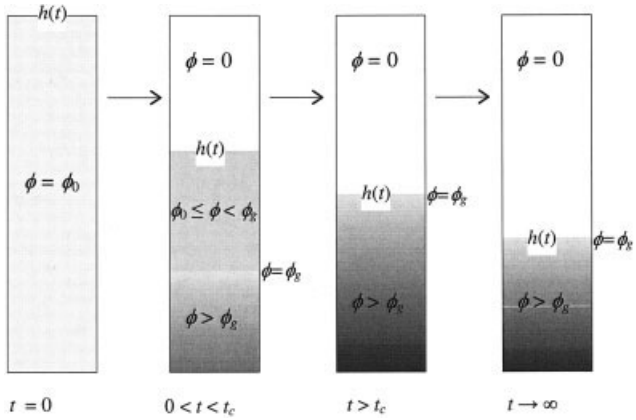


**Figure 3. Batch-settling test.**

$$\frac{\partial \phi}{\partial T} = \frac{\partial}{\partial Z}\left(\frac{D(\phi)}{LU_{sed}(\phi_g)}\frac{\partial \phi}{\partial Z} + \frac{U_{sed}(\phi)}{U_{sed}(\phi_g)}\phi\right). \quad (18)$$

Choosing

$$L = \frac{D(\phi_g)}{U_{sed}(\phi_g)}, \quad (19)$$

then

$$\frac{\partial \phi}{\partial T} = \frac{\partial}{\partial Z}\left(\Delta(\phi)\frac{\partial \phi}{\partial Z} + F(\phi)\phi\right), \quad (20)$$

where

$$F(\phi) = \frac{U_{sed}(\phi)}{U_{sed}(\phi_g)} \quad (21)$$

and

$$\Delta(\phi) = \frac{D(\phi)}{D(\phi_g)}. \quad (22)$$

In this scaling, $F(\phi_g) = \Delta(\phi_g) = 1$ and the boundary conditions become:

$$\left.\frac{\partial \phi}{\partial Z}\right|_{Z=0} = -\left.\frac{F(\phi)}{\Delta(\phi)}\phi\right|_{Z=0} \quad (23)$$

and

$$\phi(H, T) = \phi_g. \quad (24)$$

### *Infinite time solution*

At infinite time, the solids concentration distribution, $\phi(Z, T) \rightarrow \Phi(Z)$, can be determined as the solution of

$$\frac{d\Phi(Z)}{dZ} = -\frac{F(\Phi(Z))}{\Delta(\Phi(Z))}\Phi(Z) \quad (25)$$

subject to the constraint $\Phi(0) = \phi_\infty$. Note that $H_\infty = Z^*$ where $\Phi(Z^*) = \phi_g$. For large time,

$$\phi(Z, T) = \Phi(Z) + \delta\phi(Z, T). \quad (26)$$

Substitution of Eq. 26 into Eq. 20 and neglecting second order terms in $\delta\phi(Z, T)$ gives

$$\frac{\partial \delta\phi(Z, T)}{\partial T} = \frac{\partial}{\partial Z}\left(\Delta(Z)\frac{\partial \delta\phi(Z, T)}{\partial Z} + G(Z)\delta\phi(Z, T)\right) + \cdots, \quad (27)$$

where

$$\Delta(Z) = \Delta(\Phi(Z)) \quad (28)$$

and

$$G(Z) = G(\Phi(Z)) = \Delta'(\Phi(Z))\frac{d\Phi(Z)}{dZ} + F(\Phi(Z)) + F'(\Phi(Z))\Phi(Z) = F(\Phi(Z))\left[\left(\frac{F'(\Phi(Z))}{F(\Phi(Z))} - \frac{\Delta'(\Phi(Z))}{\Delta(\Phi(Z))}\right)\Phi(Z) + 1\right] \quad (29)$$

Note that $\Delta(Z)$ is zero for $Z > H_\infty$ since $\Phi(Z) < \phi_g$ here, but, as we will show, this region is not sampled.

Equation 23 leads to the boundary condition on $\delta\phi$ such that

$$\left.\frac{\partial \delta\phi(Z, T)}{\partial Z}\right|_{Z=0} + \left(\frac{G(Z)}{\Delta(Z)}\right)\delta\phi(Z, T)\Big|_{Z=0} = 0 \quad (30)$$

and Eq. 24 leads to

$$\phi_g = \Phi(H(T)) + \delta\phi(H(T), T) = \Phi(H_\infty) + \left.\frac{d\Phi}{dZ}\right|_{H_\infty}(H(T) - H_\infty) + \delta\phi(H_\infty, T) + \left.\frac{\partial \delta\phi}{\partial Z}\right|_{H_\infty}(H(T) - H_\infty) + \cdots$$

which to leading order is

$$0 = \left.\frac{d\Phi(Z)}{dZ}\right|_{H_\infty}(H(T) - H_\infty) + \delta\phi(H_\infty, T) + \cdots \quad (31)$$

where $d\Phi(Z)/dZ|_{H_\infty}$ is replaced by $-\phi_g$ from Eq. 25.

### *Solids conservation*

A material balance over the entire sediment from $Z = 0$ to $Z = H(T)$ is given by

$$\phi_0 h_0 = \int_0^{H(T)} \phi dZ = \int_0^{H_\infty} \Phi(Z)dZ + \int_{H_\infty}^{H(T)} \Phi(Z)dZ + \int_0^{H_\infty} \delta\phi(Z, T)dZ + \int_{H_\infty}^{H(T)} \delta\phi(Z, T)dZ$$

which to leading order is

$$0 = \phi_g(H(T) - H_\infty) + \int_0^{H_\infty} \delta\phi(Z, T)dZ + \cdots \quad (32)$$

### *Large time solution*

The separation of variables solution of Eq. 27 is given by

$$\delta\phi(Z, T) = \sum_{n=1}^{\infty} \delta\varphi_n(Z) e^{-\gamma_n T} \tag{33}$$

where

$$-\gamma_n \delta\varphi_n(Z) = \frac{d}{dZ}\left(\Delta(Z)\frac{d\delta\varphi_n(Z)}{dZ} + G(Z)\delta\varphi_n(Z)\right) \tag{34}$$

with the boundary conditions obtained as follows:

(i) Adding Eqs. 32 and 31 gives

$$0 = \int_0^{H_\infty} \delta\phi(Z, T)dZ + \delta\phi(H_\infty, T). \tag{35}$$

Inserting Eq. 33 and equating coefficients of $e^{-\gamma_n T}$ produces the relation

$$\delta\varphi_n(H_\infty) + \int_0^{H_\infty} \delta\varphi_n(Z)dZ = 0; \quad n = 1, 2, 3, \ldots. \tag{36}$$

(ii) Inserting Eq. 33 into 30 and equating coefficients of $e^{-\gamma_n T}$ produces the relation

$$\left[\frac{d\delta\varphi_n(Z)}{dZ} + \frac{G(Z)}{\Delta(Z)}\delta\varphi_n(Z)\right]_{Z=0} = 0; \quad n = 1, 2, 3, \cdots \tag{37}$$

### *Eigenvalue problem*

Determination of $\gamma_n$ and $\delta\varphi_n(Z)$ requires finding the solutions of

$$-\gamma\delta\varphi(Z) = \frac{d}{dZ}\left(\Delta(Z)\frac{d\delta\varphi(Z)}{dZ} + G(Z)\delta\varphi(Z)\right) \tag{38}$$

subject to

$$\delta\varphi(H_\infty) + \int_0^{H_\infty} \delta\varphi(Z)dZ = 0 \tag{39}$$

and

$$\left[\frac{d\delta\varphi(Z)}{dZ} + \frac{G(Z)}{\Delta(Z)}\delta\varphi(Z)\right]_{Z=0} = 0. \tag{40}$$

The eigenvalues are ranked so that $\gamma_1$ is smallest. Re-arranging Eq. 31, we obtain

$$H(T) - H_\infty = \frac{\delta\phi(H_\infty, T)}{\phi_g}, \tag{41}$$

which leads to

$$H(T) - H_\infty = \frac{\sum_{n=1}^{\infty} \delta\varphi_n(H_\infty)e^{-\gamma_n T}}{\phi_g}. \tag{42}$$

Thus

$$H(T) - H_\infty = \frac{\delta\varphi_1(H_\infty)}{\phi_g} e^{-\gamma_1 T} + \frac{\delta\varphi_2(H_\infty)}{\phi_g} e^{-\gamma_2 T} + \cdots \tag{43}$$

Given the large expected difference between $\gamma_1$ and $\gamma_2$, Eq. 43 can be truncated to its first term without discernable loss of accuracy to give

$$H(T) - H_\infty = \frac{\delta\varphi_1(H_\infty)}{\phi_g} e^{-\gamma_1 T}. \tag{44}$$

In the absence of a suitable initial condition on $\delta\phi(Z, T)$, $\delta\varphi_1(H_\infty)$ is only determined to within a multiplicative constant. We can write in the unscaled form

$$h(t) - h_\infty = \exp\left(A - \frac{U_{sed}(\phi_g)}{L}\gamma_1 t\right), \tag{45}$$

where $A$ is an undefined constant. Given that this analysis is expected to be valid from the critical time, $t_c$, when $\phi(h(t_c), t_c) = \phi_g$, if this critical time and the corresponding height, $(t_c, h(t_c))$, are known, then $A$ can be determined from

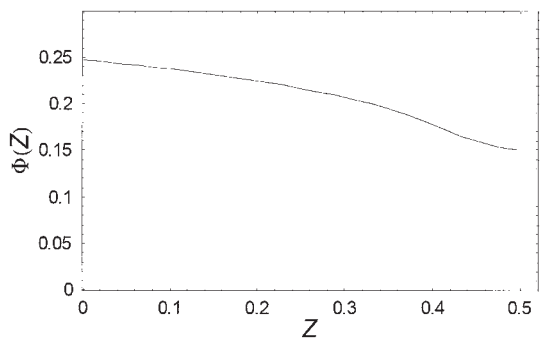


**Figure 4. Predicted equilibrium solids volume fraction distribution for batch-settling test with initial height of 1 m and an initial solids volume fraction of 0.1.**

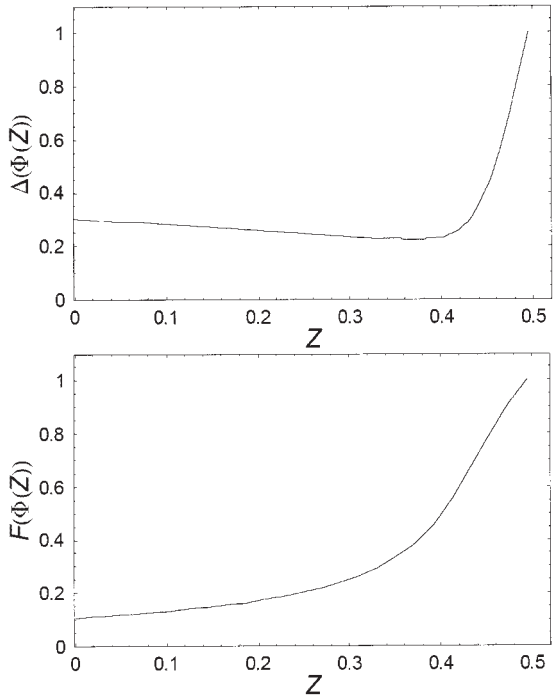


**Figure 5. Predicted equilibrium function distributions $\Delta(\Phi(Z))$ and $F(\Phi(Z))$ for a batch-settling test with initial height of 1 m and an initial solids volume fraction of 0.1.**

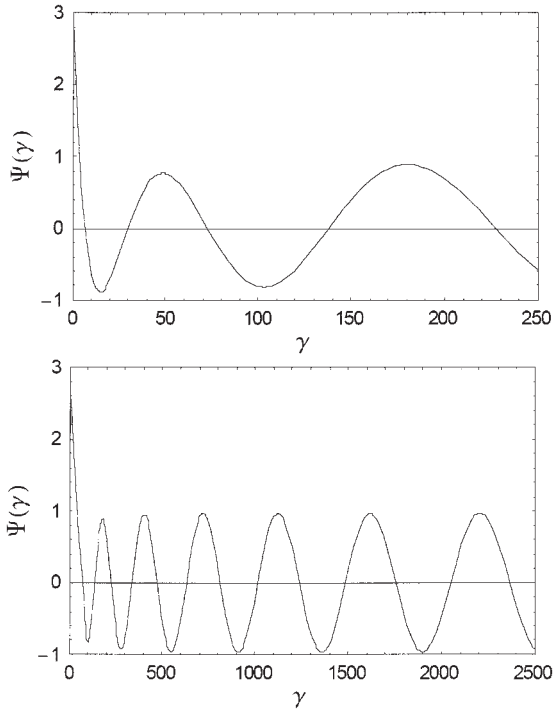


**Figure 6. Predicted determinant $\psi(\gamma)$ for a batch-settling test with initial height of 1 m and an initial solids volume fraction of 0.1.**

$$A = \ln(h(t_c) - h_\infty) + \frac{U_{sed}(\phi_g)}{L}\gamma_1 t_c. \tag{46}$$

### *Numerical solution*

Numerical solution involves first picking a value of $\gamma$ and then finding two linearly independent solutions of Eq. 38: $\delta\varphi^{(1)}(Z)$ and $\delta\varphi^{(2)}(Z)$, such that

$$\begin{cases} \delta\varphi^{(1)}(0) = 0 \\ \dfrac{\partial}{\partial Z}\delta\varphi^{(1)}(0) = 1 \end{cases} \quad \text{and} \quad \begin{cases} \delta\varphi^{(2)}(0) = 1 \\ \dfrac{\partial}{\partial Z}\delta\varphi^{(2)}(0) = 0 \end{cases}.$$

The general solution is

$$\delta\varphi(Z) = C^{(1)}\delta\varphi^{(1)}(Z) + C^{(2)}\delta\varphi^{(2)}(Z) \tag{47}$$

with $C^{(1)}$ and $C^{(2)}$ chosen to satisfy the boundary conditions in Eqs. 39 and 40.

Substituting Eq. 47 into 40 leads to

$$C^{(1)} + C^{(2)}\left(\frac{G(0)}{\Delta(0)}\right) = 0. \tag{48}$$

Substituting Eq. 47 into 39 leads to

$$C^{(1)}\left[\delta\varphi^{(1)}(H_\infty) + \int_0^{H_\infty}\delta\varphi^{(1)}(Z)dZ\right] + C^{(2)}\left[\delta\varphi^{(2)}(H_\infty) + \int_0^{H_\infty}\delta\varphi^{(2)}(Z)dZ\right] = 0, \tag{49}$$

Thus we have

$$\begin{pmatrix} 1 & \left(\dfrac{G(0)}{\Delta(0)}\right) \\ \left[\delta\varphi^{(1)}(H_\infty) + \displaystyle\int_0^{H_\infty}\delta\varphi^{(1)}(Z)dZ\right] & \left[\delta\varphi^{(2)}(H_\infty) + \displaystyle\int_0^{H_\infty}\delta\varphi^{(2)}(Z)dZ\right] \end{pmatrix} \begin{pmatrix} C^{(1)} \\ C^{(2)} \end{pmatrix} = \begin{pmatrix} 0 \\ 0 \end{pmatrix}. \tag{50}$$

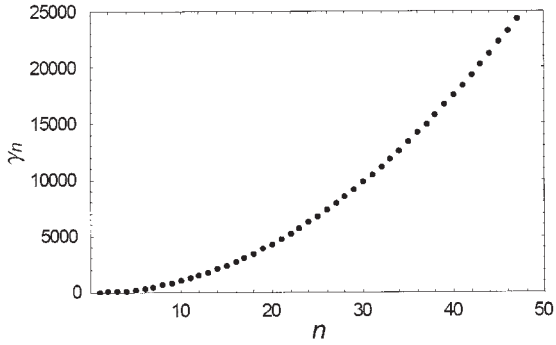


**Figure 7. Predicted eigenvalues, $\gamma_n$, for a batch-settling test with initial height of 1 m and an initial solids volume fraction of 0.1.**

The determinant of the coefficient matrix,

$$\Psi(\gamma) = \left[ \delta\varphi^{(2)}(H_\infty) + \int_0^{H_\infty} \delta\varphi^{(2)}(Z)dZ \right] - \left( \frac{G(0)}{\Delta(0)} \right) \left[ \delta\varphi^{(1)}(H_\infty) + \int_0^{H_\infty} \delta\varphi^{(1)}(Z)dZ \right]. \quad (51)$$

For a non-trivial solution, we require that $\Psi(\gamma) = 0$.

## Example

### *Eigenvalue determination*

Using the functional forms described in Figures 1 and 2, the function $\psi(\gamma)$ was determined for a batch-settling test with an initial height of 1 m and an initial solids volume fraction of 0.1. An assumed solids density $\rho_{sol} = 3200$ kg m$^{-3}$ and a liquid density $\rho_{liq} = 1000$ kg m$^{-3}$ give a solid-liquid density difference $\Delta\rho = 2200$ kg m$^{-3}$. From Eq. 19, $L$ was determined to be 0.96488. The scaled equilibrium solids concentration distribution, $\Phi(Z)$, shown in Figure 4, was determined using Eq. 25, and the scaled final height, $H_f$, was determined to be 0.49452. The scaled diffusivity function, $\Delta(\phi) = D(\phi)/D(\phi_g)$ from Eq. 22, was determined for the equilibrium solids concentration distribution, $\Phi(Z)$, to produce $\Delta(\Phi(Z))$, as shown in Figure 5. The scaled sedimentation velocity function, $F(\phi) = U_{sed}(\phi)/U_{sed}(\phi_g)$ from Eq. 21, was also determined for the equilibrium solids concentration distribution, $\Phi(Z)$, to produce $F(\Phi(Z))$, as shown in Figure 5. The equilibrium function $G(\Phi(Z))$ was determined from Eq. 29 using $\Phi(Z)$, $\Delta(\Phi(Z))$, and $F(\Phi(Z))$ as inputs. The determinant $\Psi(\gamma)$, shown in Figure 6, was calculated from $\gamma = 0$ to 25,000 and is bounded by the range $(-1,1)$ for all $\gamma > 10$. The eigenvalues, $\gamma_n$, where $\Psi(\gamma_n) = 0$, were determined for $n = 1$ to 47 (with $\gamma_1 = 6.6270$, $\gamma_2 = 29.8692$, etc.), as shown in Figure 7. The functional behavior of $\gamma_n$, though not analytically defined, is related to $(n - 1/2)^2$ as $n$ becomes large, as demonstrated by the plot of $\gamma_n/(n - 1/2)^2$ versus $n$ in Figure 8. Knowledge of this relationship can be useful when searching for eigenvalues. Since the second and subsequent eigenvalues, $(\gamma_2, \gamma_3 \ldots)$, are all much larger than $\gamma_1$, only the first term of the infinite series in Eq. 43 is anticipated to be significant

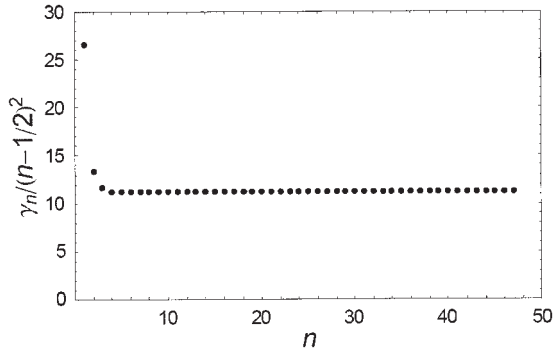


**Figure 8. Predicted values of $\gamma_n/(n - 1/2)^2$ for a batch-settling test with initial height of 1 m and an initial solids volume fraction of 0.1.**

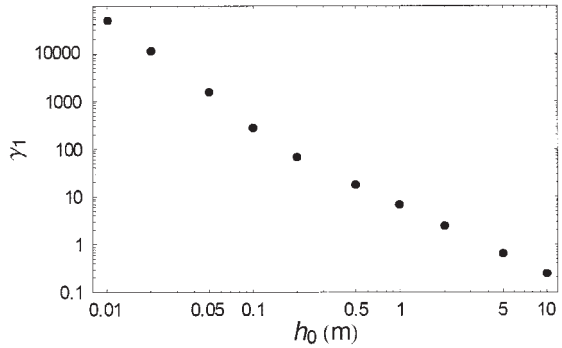


**Figure 9. Predicted values of $\gamma_1$ for batch-settling tests with a variable initial height and an initial solids volume fraction of 0.1.**

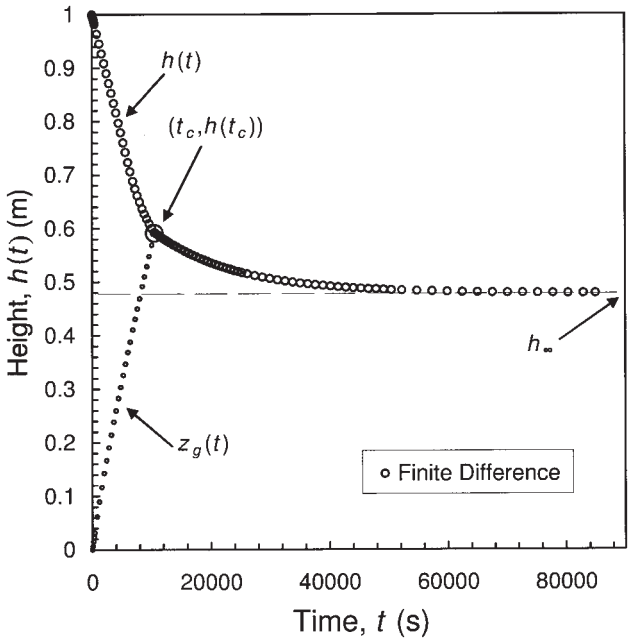


**Figure 10. Plot of numerical finite-difference predictions of the sediment-interface height, $h(t)$, and the gel point height, $z_g(t)$, for batch-settling tests with an initial height of 1 m and an initial solids volume fraction of 0.1.**

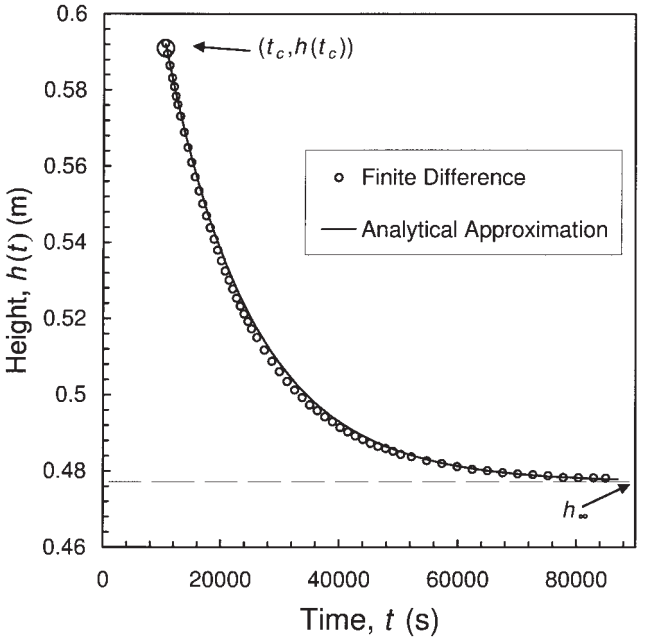


**Figure 11. Focused plot of numerical finite-difference predictions and analytical approximation of the sediment-interface height, $h(t)$, for batch-settling tests with an initial height of 1 m and an initial solids volume fraction of 0.1.**

at large times, justifying the series truncation in Eq. 44. The variability of $\gamma_1$ with the initial suspension height, $h_0$, shown in Figure 9, is loosely proportional to $h_0^{-2}$. This correlation is not strong enough for accurate extrapolation, but this loose relationship can be used to produce an initial guess for $\gamma_1$ when $h_0$ is varied.

### *Sediment-interface height prediction*

A numerical prediction of $h(t)$ for the case of an initial height of 1 m and an initial solids volume fraction of 0.1 has been determined using an explicit finite difference algorithm similar to those described by Bürger and Karlsen.[3] The computation utilized a resolution of 1000 height elements and 24 incremental time steps per second, requiring over 54 hours of computation time using a 3GHz Pentium 4™ processor. Predictions of the sediment-interface height, $h(t)$, and the gel point height, $z_g(t)$, are shown in Figure 10, along with the highlighted critical point $(t_c, h(t_c)) = (10500, 0.591)$. Using this critical point to determine $A = -1.4708$, Eq. 45 becomes

$$h(t) = 0.4772 + \exp(-1.4708 - 6.6866 \times 10^{-5} t) : t > t_c. \tag{52}$$

A focused plot of the finite element prediction compared with the analytical approximation in Eq. 52 is plotted in Figure 11, demonstrating an excellent correlation.

The numerical analysis presented here demonstrates the potential to accurately predict $h(t)$ for long time without the exhaustive level of computation required in numerical algorithms that are discretized in time. A new more computationally efficient methodology for the prediction of $h(t)$ for all time would involve two parts:

(i) For $0 \le t \le t_c$, a numerical prediction of $h(t)$ until $z_g'(t) = 0$ at the critical time $t_c$ using a finite element or Runge-Kutta method that is discretized in time.

(ii) For $t > t_c$, a numerical determination of $\gamma_1$ as the lowest positive solution $\gamma$ to the equation $\Psi(\gamma) = 0$ (see Eq. 51), used with $(t_c, h(t_c))$ in Eq. 46 to determine $A$. The behavior of $h(t)$ is then described by Eq. 45.

## Conclusions

A simple analytical approximation has been derived to describe long-time batch-settling behavior along with a numerical method for determining the equation parameters. The analytical approximation has been shown to compare favorably with finite element predictions. This new knowledge has the potential to significantly reduce the computational time requirements of predicting long-time batch-settling behavior.

## Acknowledgments

The financial support of the Particulate Fluids Processing Centre, a Special Research Centre of the Australian Research Council (ARC), and an ARC Discovery Project is acknowledged.

## Literature Cited

1. Lester DR, Usher SP, Scales PJ. Estimation of the hindered settling function $R(\phi)$ from batch-settling tests. *AIChE J.* 2005;51(4):1158-1168.
2. Lester DR. Colloidal suspension dewatering analysis. Ph.D. thesis, The University of Melbourne, Melbourne, Australia, 2002.
3. Bürger R, Karlsen KH. On some upwind difference schemes for the phenomenological sedimentation-consolidation model. *J Eng Math.* 2001;41:145-166.
4. Howells I, Landman KA, Panjkov A, Sirakoff C, White LR. Time dependent batch settling of flocculated suspensions. *Appl Math Model.* 1990;14:77-86.
5. Roberts EJ. Thickening—art or science? *Mining Transactions.* 1949; 184:61-64.
6. Fitch B. Thickening theories—an analysis. *AIChE J.* 1993;39(1):27-36.
7. Behn VC. Settling behaviour of waste suspensions. *Journal of the Sanitary Engineering Division, Proceedings of the American Society of Civil Engineers*. 1957;83(SA5):1423–1-20.
8. Landman KA, White LR. Predicting filtration time and maximizing throughput in a pressure filter. *AIChE J.* 1997;43(12):3147-3160.
9. de Kretser RG, Scales PJ, Boger DV. Compressive rheology: an overview. In *Rheology Reviews 2003*, Binding DM, Walters K, Eds. Aberystwyth: British Society of Rheology; 2003. pp 125-166.
10. Green MD. Characterisation of suspensions in settling and compression. Ph.D. thesis, The University of Melbourne, Melbourne, Australia, 1997.
11. Green MD, Landman KA, de Kretser RG, Boger DV. Pressure filtration technique for complete characterization of consolidating suspensions. *Industrial Engineering and Chemistry Research.* 1998;37(10): 4152-4156.
12. Usher SP. Suspension dewatering: characterisation and optimisation. Ph.D. thesis, The University of Melbourne, Melbourne, Australia, 2002.
13. Usher SP, de Kretser RG, Scales PJ. Validation of a new filtration technique for dewaterability characterization. *AIChE J.* 2001;47(7): 1561-1570.
14. de Kretser RG, Usher SP, Scales PJ, Boger DV, Landman KA. Rapid filtration measurement of dewatering design and optimization parameters. *AIChE J.* 2001;47(8):1758-1769.
15. Landman KA, White LR, Buscall R. The continuous flow gravity thickener: steady state behaviour. *AIChE J.* 1988;34(2):239-252.

*Manuscript received Feb. 28, 2005, and revision received Aug. 31, 2005.*